

Journal of Materials Chemistry A

Accepted Manuscript



This is an *Accepted Manuscript*, which has been through the Royal Society of Chemistry peer review process and has been accepted for publication.

Accepted Manuscripts are published online shortly after acceptance, before technical editing, formatting and proof reading. Using this free service, authors can make their results available to the community, in citable form, before we publish the edited article. We will replace this *Accepted Manuscript* with the edited and formatted *Advance Article* as soon as it is available.

You can find more information about *Accepted Manuscripts* in the [Information for Authors](#).

Please note that technical editing may introduce minor changes to the text and/or graphics, which may alter content. The journal's standard [Terms & Conditions](#) and the [Ethical guidelines](#) still apply. In no event shall the Royal Society of Chemistry be held responsible for any errors or omissions in this *Accepted Manuscript* or any consequences arising from the use of any information it contains.

Cite this: DOI: 10.1039/c0xx00000x

www.rsc.org/xxxxxx

Low temperature sintering of binder-containing TiO₂/metal peroxide pastes for dye-sensitized solar cells

Peter J. Holliman^{a,b}, Dhiyaa K. Muslem^a, Eurig W. Jones^a, Arthur Connell^a, Matthew L. Davies^a, Cecile Charboneau^b, Matthew J. Carnie^b and David A. Worsley^b

Received (in XXX, XXX) Xth XXXXXXXXXX 20XX, Accepted Xth XXXXXXXXXX 20XX
DOI: 10.1039/b000000x

Nano-structured metal oxide films are a key component of dye-sensitized (DSC) solar cells. Scaling such devices requires lower temperature processing to enable cheaper substrates to be used. In this context, we report a new and scaleable method to sinter binder-containing metal oxide pastes to make DSC photo-electrodes at lower temperatures. Metal peroxide powders (CaO₂, MgO₂, or ZnO₂) have been added to terpeneol-based P25 pastes containing ethyl cellulose binder or to commercial TiO₂ paste (DSL18NR-T). Thermal analysis shows binder decomposition occurring at 300 °C instead of the standard 450 °C for a TiO₂-only paste and suggests that the metal peroxides act as combustion promoters releasing heat and oxygen within the film at temperatures. The data show that this heat and oxygen release coincide best with binder combustion for ZnO₂ and DSC device tests show that adding ZnO₂ to TiO₂ pastes produces the best performances affording $\eta = 7.5\%$ for small devices (0.26 cm²) and $\eta = 5.7\%$ at 300 °C or 450 °C for DSL18NR-T/ZnO₂ for larger (1 cm²) devices. To the best of our knowledge, the performance of the (0.26 cm²) cells is comparable to the highest efficiency devices reported for DSC fabricated using low temperature methods. Device efficiency was most strongly linked with J_{sc}, BET and dye sorption measurements suggesting that J_{sc} was linked with metal oxide surface area and dye loading. The latter was linked to the availability of surface sorption sites for dye molecules which was strongly negatively affected by any residual organic binder which resulted from incomplete combustion.

O'Regan and Grätzel's breakthrough in dye-sensitised solar cell (DSC) technology¹ showed that sintering pre-made TiO₂ nano-crystals²⁻⁴ at 450-600 °C significantly increases the photo-anode surface area, dye loading and short circuit current. This has led to considerable interest in DSC devices as promising candidates for large scale, low cost PV because they should be manufacturable using printing and roll-to-roll processing using abundant and non-toxic raw materials^{5,6}.

In DSC devices, the mechanical and electrical connectivity between the TiO₂ particles are key to long-term device function as charge must travel through the photo-electrode to the current collecting working electrode⁷. Typically this is achieved by printing a colloidal suspension of well-dispersed, crystalline TiO₂ nanoparticles where the paste rheology is controlled by the addition of a long-chain organic polymer (the binder). The binder enables crack-free films to be printed with variable but controlled films thicknesses at a range of scales. Without the binder present, it is impossible to print large enough photo-electrodes to scale the technology. This means that currently printed films must be sintered at > 450 °C to completely combust the organic binder to free up dye sorption sites on the surface of the TiO₂ particles and to enable robust inter-particle connections to form but low

enough to minimise any reduction in TiO₂ surface area. However, this limits the working electrode substrate to FTO-coated glass or Ti foil⁸ which are inflexible and heavy or expensive⁹, respectively. By comparison cheaper, more lightweight and flexible substrates which are suitable for large-scale roll-to-roll manufacture (e.g. metal foils, TCO-coated plastic) require lower processing temperatures; typically 300 °C for metal foils and 150 °C for plastics¹⁰. However, there are no reports in the literature to date of methods to sinter binder-containing pastes at low temperature.

Instead, although low temperature sintering of photo-anodes for DSC has been widely studied, reports have centred on using binder-free pastes. However, as discussed previously, binder-free pastes are significantly limited for larger scale applications because of the difficulties in controlling printability and film consistency over wider areas (e.g. film thickness, and inter-particle adhesion which can lead to cracking and substrate adhesion which can lead to delamination). Binder-free approaches have included spin coating¹¹, sol gel¹², hydrothermal treatment¹³⁻¹⁵ chemical sintering¹⁶⁻¹⁷, pressure sintering¹⁸⁻²⁰, electrophoretic deposition of TiO₂ nanoparticles²¹, varying TiO₂ particles²² and the use of electron beam showers²³. Variations on

radiant heating have also been studied including laser treatment²⁴, microwave irradiation²⁵ and post-sintering O₂ plasma²⁶ aimed at removing residual organic matter from the metal oxide surface. Whilst these approaches have shown promise at the laboratory

scale, producing consistent, large-scale meso-porous films required for DSC device manufacturing will require the presence of a binder in the TiO₂ colloid. Hence, the study of low temperature approaches to sintering binder-containing metal oxide pastes remains a key challenge for DSC manufacturing.

In this context, this paper reports a new approach to lower sintering temperatures of binder-containing metal oxide pastes to manufacture photo-electrodes for DSC. We believe this is the first report using solid peroxides as combustion promoters. This approach enables accurate control of paste rheology by retaining an organic polymer binder in the metal oxide pastes which is essential to produce coherent, large scale films with consistent thickness. Our combined experimental approach has been to screen larger films (3 x 2 cm) to examine film coherence and colour, to understand the fundamental thermal chemistry of screen printing pastes and how this influences sintering and then to make larger DSC devices than are typically reported (1 cm²) to test the effects of sintering on performance. Finally, we have studied metal oxide area and dye loading to investigate the links between short circuit current and sintering treatment.

Experimental

Paste and device manufacture

P25 pastes were prepared by thoroughly mixing P25 (16 g, Degussa) with terpineol (64.9 g, Fluka) and ethyl cellulose (8 g, Fluka Product# 46070). Peroxide containing pastes were prepared by adding calcium peroxide, magnesium peroxide or zinc peroxide (10% w/w *versus* TiO₂, all Aldrich) and thoroughly mixing for 1 h. Commercial DSL18NR-T paste (Dyesol) was either used as purchased or metal peroxide was added as described above.

Photo-electrodes were prepared prepared by doctor blading metal oxide paste on to FTO-coated glass (TEC15, NSG) and sintering in air at either 450 °C, 300 °C or 150 °C for 30min. Larger films were prepared (3 x 2 cm) to study film coherence over a larger area. DSC devices were prepared using 1 cm² films (minimum 3 replicates per treatment) to study film coherence and reproducibility. Selected films were then immersed in 40 mM TiCl₄:THF_{2(aq)} at 70 °C for 30min before rinsing with water and air drying for 10min. The films were then re-sintered at the same temperature used during the first sintering process so that no film experienced a temperature greater than its initial sintering temperature at any point during processing.

Counter electrodes were prepared by spreading PT1 paste (Dyesol) on to TEC 8 glass (NSG) and heating to 400 °C in air for 30min. The photo and counter electrodes were then sealed together using a Surlyn gasket at 120 °C followed by fast dyeing with 0.3 mM N719 (Dyesol) in acetonitrile:*tert.*-butanol (1:1 v/v) for 10min as described previously.²⁷ The electrolyte was 0.8 M 1-methyl-3-propyl imidazolium iodide, 0.05 M *tert.*-butyl ammonium iodide, 0.05 M I₂, 0.3 M benzimidazole and 0.05 M guanidinium thiocyanate in acetonitrile.

Device Characterisation

Current-voltage characteristics were measured using an ABET Solar Simulator with Xe arc lamp and a Keithley 2400 at 100 mW cm⁻² or 1 Sun between 0 and 1 V. Spectral response was measured from 300-800 nm on a QEX10 Quantum Efficiency Measurement System in DC mode at resolution of 10 nm. Lamps were calibrated to 1 Sun (100 mW cm⁻²) using a certified (Oriel 91150V) mono-crystalline Si reference cell traceable to the National Renewable Energy Laboratory (NREL).

Photocurrent and photovoltage transients were measured as described in²⁸. The white bias light was provided by a BRIDGELUX 9000 lumen LED array (Farnell) whilst the pulse light was provided by a bank of four OSLO PowerCluster green LED arrays (RS). Pulse intensity was chosen to make sure $\Delta V < 10$ mV above V_{OC}. A pulse length of 250 μ s was utilized and was generated *via* a fast MOSFET transistor controlled by a National Instruments USB-6251 data acquisition board (DAQ) and WaveMetrics IGOR Pro software. Voltages were measured directly using the DAQ whilst currents were measured *via* a voltage drop against a 1 Ω resistor.

XRD was carried out using a PANalytical diffractometer at 45 kV and 35 mA between 20 and 60° 2 θ using Ni-filtered Cu-K _{α} 1 radiation ($\lambda=1.5405$ Å). Thermal gravimetric analysis and differential scanning calorimetry were performed using a SDTQ600 TGA/DSC (TA Instruments Ltd). The pastes were either run as prepared or were pre-dried at 100-110 °C for 2 h to evaporate the solvent to focus the analysis on binder combustion. The samples were ramped at 10 °C min⁻¹ between room temperature and 600 °C under flowing air. Surface area of pre-sintered doctor-bladed films was determined using BET (Brunauer-Emmett-Teller) isotherms at -196 °C using a Micromeritics Gemini III 2375. Electron microscopy and energy dispersive X-ray elemental analyses were performed on a Field Emission Gun-Scanning Electron Microscope (FEG-SEM) Hitachi S-4800 (12 keV, 10 μ A) equipped with an Oxford instruments X-Max (50 mm² window) detector.

N719 dye sorption was studied using sintered P25 and P25/ZnO₂ films either by directly immersing the film in N719 dye solution for 24 h or by scraping sintered films off a glass substrate and immersing the collected powder into N719 dye solution for 24 h. N719 uptake was quantified by firstly desorbing the dye using 0.1 M NaOH_(aq)/ ethanol (1:1 v/v) followed by calculation of the concentration of the desorbed solution using UV-visible spectroscopy at 512 nm in conjunction with a calibration graph (see ESI Fig. 1) obtained by using six N719 standards from 0 to 1.0 mM (11.82 mM⁻¹cm⁻¹)²⁹.

Equilibrium N719 adsorption capacity of N719 was measured for freely-dispersed P25, P25/ZnO₂ powder at seven N719 concentrations (25-500 mg/l) at 22, 40 and 50 °C. Adsorbed dye (q) (mg/g) was calculated according to Eqn. 1³⁰

$$q = (C_0 - C_e) V/m \quad (\text{Eq. 1})$$

where C₀ (mg/L) and C_e (mg/L) are the initial and equilibrium N719 concentrations (mol L⁻¹), respectively, V is the volume of dye solution (L), and m is the mass TiO₂ (mg). Fits to the Langmuir (Eq. 2)³¹ or Freundlich isotherms (Eq. 3 and 4)^{31,32}

were then calculated by plotting the data according to the relevant equations. For Langmuir,

$$C_e/q = 1/K_L q_m + C_e/q_m \quad (\text{Eq. 2})$$

where C_e is the equilibrium N719 concentration (mg/l), q is the equilibrium adsorption capacity (mg/g), q_m is the maximum adsorption capacity (mg/g) and K_L (L/mg) is the Langmuir constant. For Freundlich, Eq. 3 was converted to the linear form (Eq. 4).

$$q_e = K_f C_e^{1/n} \quad (\text{Eq. 3})$$

$$\ln q_e = \ln K_f + 1/n \ln C_e \quad (\text{Eq. 4})$$

where q_e is the equilibrium adsorbate concentration (mg/g), K_f is the Freundlich constant (mg/g), C_e is the equilibrium solution concentration (mg/l), and $1/n$ represents dimensionless heterogeneity factor.

Results and Discussion

To emphasise the importance of the binder within the pastes, two P25/terpineol pastes were prepared; one with ethyl cellulose binder and one without. These were doctor bladed onto glass microscope slides and oven sintered at 450 °C for 30min. Fig. 1 initially suggests that the resultant films appear similar. However, closer inspection of the binder-free film reveals fine cracks and a simple adhesion test of applying Scotch tape to the film and removing it shows that the TiO_2 arising from the binder-free paste delaminates easily (as denoted by the dashed red box on Fig. 1) whilst the film from the binder-containing paste remains strongly adhered to the glass substrate.

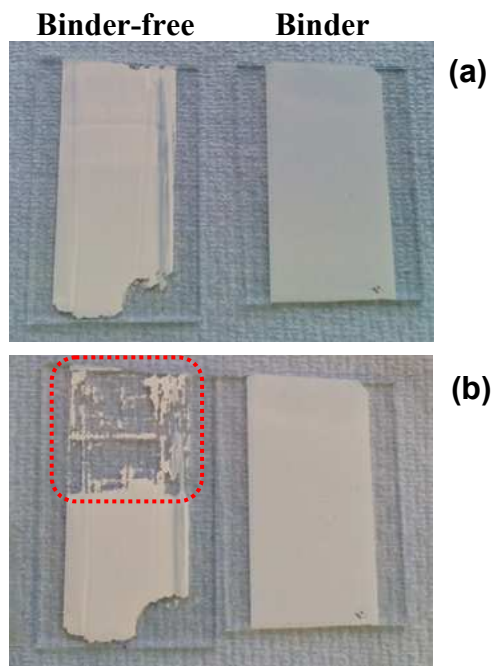


Fig. 1 Photographs of films produced by sintering either binder-free or binder-containing P25 pastes at 450 °C for 30min; (a) as produced films and (b) after adhesion test using Scotch tape. Binder = ethyl cellulose

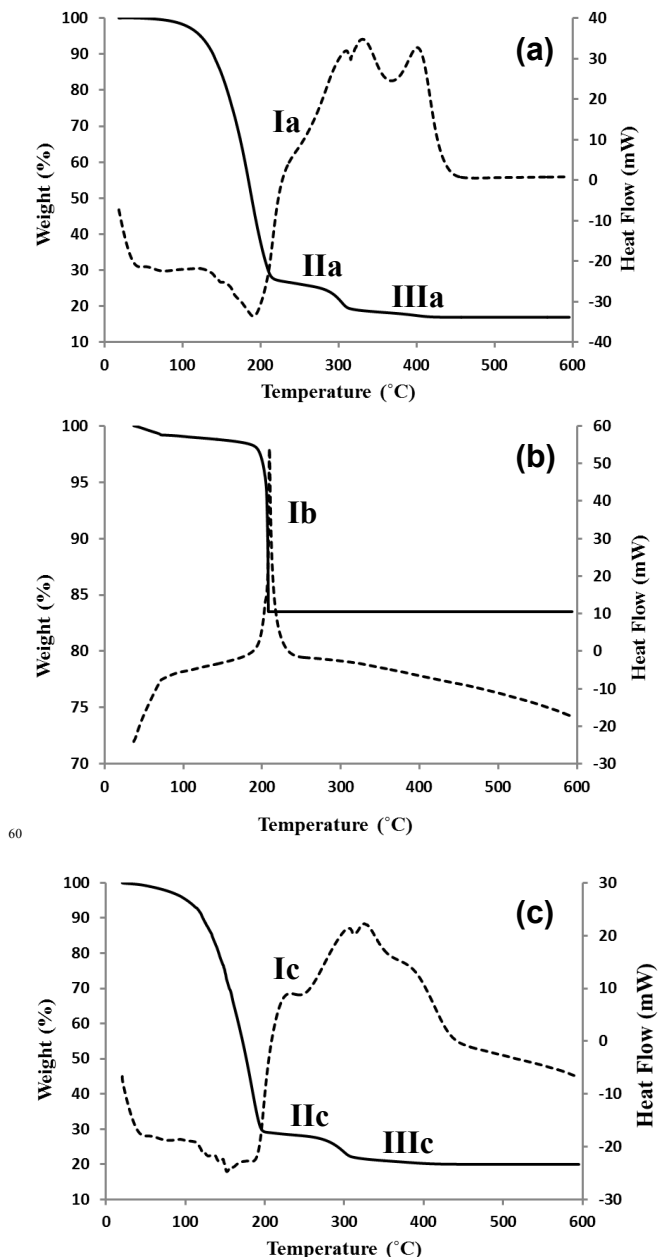


Fig. 2 TGA/DSC data for (a) P25 paste, (b) ZnO_2 powder and (c) P25/ ZnO_2 paste heated from RT to 600 °C at 10 °C min⁻¹. TGA = solid lines and DSC = dashed lines. Exotherm = up

Thermal chemistry

The approach taken in this paper is to lower the sintering temperature of binder-containing pastes by including metal peroxide powders which decompose to produce metal oxide particles and release oxygen and heat within the photo-electrode film during the sintering process.

Detailed thermal analyses of selected pastes used in this study are shown in Fig. 2 (all the data are shown in the ESI Fig. 2). These TGA/DSC data can be used to explain the principle of the metal peroxide combustion effect. In addition, the challenge of lowering the sintering temperature of metal oxide pastes can be seen by looking at the detailed thermal analysis of a P25 paste (Fig. 2a). The data show a three-stage weight loss for P25-only

pastes with an initial loss of terpineol solvent (*ca.* 70%) between 60 °C and 214 °C which is associated with an endothermic peak which reaches its minimum at *ca.* 190 °C in line with this being an evaporative rather than a combustion process. The second weight loss (*ca.* 10%, 210-320 °C) is associated with a broad, multi-feature exotherm with a shoulder at *ca.* 240 °C (labelled **Ia** on Fig 2a) and two maxima *ca.* 290 and 320 °C. These features are associated with the combustion of ethyl cellulose to CO_{2(g)} and H₂O_(g). Although the final weight loss is small (3%, 320-450 °C), it is associated with a strong exothermic peaks (maximum at *ca.* 410 °C) which continues up to 450 °C (labelled **IIIa** in Fig. 2a). This is ascribed to the combustion of residual carbonaceous material from the ethyl cellulose binder which, if not combusted, is believed to reduce dye uptake by blocking surface sorption sites. This residual organic matter gives rise to the brown colouration in under-sintered films (see Fig. 3). It is key to remove this material to prepare suitable metal oxide surfaces for dyeing. The reason for adding the metal peroxides to the paste is to introduce an oxygen source and heat during binder combustion to accelerate the removal of this residual organic matter.

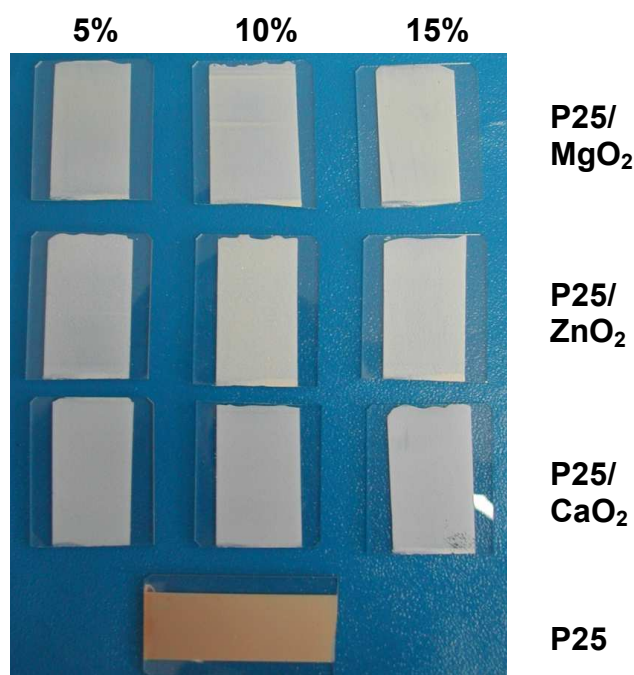
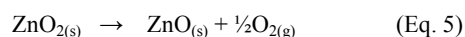


Fig. 3 Photograph of films (*ca.* 3x2 cm) prepared from P25 and P25/peroxides (5-15% w/w) binder-containing pastes after sintering for 30min at 300 °C

As such, an initial screening of P25 pastes containing metal peroxides involved mixing either calcium, magnesium or zinc peroxide into a P25/terpineol paste containing ethyl cellulose binder at a loading of 5, 10 or 15% by wt *versus* P25. After casting onto glass slides, the films were sintered up to 250-300 °C for 30-120min. Fig. 3 shows that, after 30 min at 300 °C, the P25 control film changes from yellow to brown. Further tests show that the P25-only film becomes white only after heating to 450 °C; this colour change was deemed a suitable visual indicator of complete binder combustion which would prepare the metal

oxide surface area for dyeing. The films from the metal peroxide pastes all show some residual pale brown colour at combustion temperatures up to 250 °C regardless of the metal peroxide loading (see ESI Fig. 3). At 250 °C, the P25/CaO₂ film appeared paler than the other films after 30 min but increasing the sintering time up to 120min did not change this. However, sintering these films at 300 °C for 30min produces white films for all the P25/peroxide films whilst the P25-only control remains brown (Fig. 3). Hence, 300 °C was considered to be the threshold temperature to initiate both metal peroxide decomposition (MO₂ becoming MO and ½O₂) and binder combustion.

To explore the reasons for the beneficial effects of metal peroxide in detail, further TGA/DSC data have been recorded. All the data are presented in the ESI Fig. 2 whilst only the selected data for ZnO₂ are presented here as these data are representative of all the different metal peroxides tested. Thus, TGA/DSC data for powdered ZnO₂ (Fig. 2b) show a small weight loss (*ca.* 2%) for up to 190 °C and then a very rapid weight loss of *ca.* 16% centred around 200 °C which corresponds to the decomposition of ZnO₂ into ZnO (Eq. 5). This is accompanied by a sharp exotherm which is labelled **Ib** in Fig. 2b. This is important because the ZnO₂ decomposition occurs at a slightly lower temperature than the temperature at which binder combustion commences (see **IIa** in Fig. 2a). This means that the heat or oxygen released from ZnO₂ decomposition will be available to enhance binder combustion at lower temperatures. In addition, because the metal peroxide particles are mixed into the pastes, they are subsequently distributed through the printed and sintering films. Hence, as the metal peroxides decompose, they release oxygen and heat to their local environment where the binder residues exist. This reduces any mass transfer issues which further helps to explain the enhanced binder combustion at lower temperatures.



These effects are illustrated by the data for a P25/ZnO₂ paste (Fig. 2c). As expected, the data show a very similar pattern to the P25 paste because the paste only contains 10% ZnO₂. However, there is a much more clearly defined and more intense exothermic peak in the DSC signal (labelled **Ic** on Fig. 2c). This reflects the exotherm associated with ZnO₂ decomposition. As predicted, this is believed to have two main effects; firstly additional and localized heat is released within the film and secondly the peroxide decomposing releases oxygen into the film which can help to oxidize the organic binder. This results in a greater loss of residual organic matter from the film at temperatures lower than 450 °C (labelled **IIIc** in Fig. 2c). By comparison, the TGA/DSC data for CaO₂ and MgO₂ (see ESI Fig. 2) show that, while they do decompose to produce CaO and MgO, respectively and to release oxygen, the main weight loss takes place at higher temperature (*ca.* 400 °C). Also, for both CaO₂ and MgO₂, their decomposition is an endothermic process which will remove energy from the surrounding paste during sintering. Thus, for these peroxides, the localized addition of oxygen should still occur at similar temperatures to binder combustion and therefore should still help this process. However, during any sintering process, the paste

must be heated from room temperature to the sintering dwell temperature. Hence, the higher decomposition temperatures for CaO₂ and MgO₂ means that the oxygen will be released slightly later in the process. Overall, both the higher temperature and endothermic nature of the decomposition mean that CaO₂ and MgO₂ should be less effective combustion additives compared to ZnO₂.

Having established that the addition of metal peroxides can reduce the sintering temperature of TiO₂-ethyl cellulose pastes, selected films were sintered at different temperatures and sensitized with N719 before being manufactured into dye-sensitized solar cell devices as described in the next section.

DSC device data

In this paper, we are studying sintering so we have made larger photo-electrodes (1 cm²) than are typically reported for DSC devices to test film cohesion in devices.³³ To study reproducibility, we have also made replicate devices and reported the average $\eta \pm$ the error. Whilst this suppresses device efficiencies relative to the highest efficiencies reported in the literature (e.g. for ball-milled P25 pastes^{34,35}), this approach is necessary to accurately test the effectiveness of the different sintering treatments.

Table 1 shows IV data for replicate devices made using one layer of metal oxide paste (*ca.* 7 μ m thickness) after sintering at 300 or 450 °C. The approach taken was to keep photo-electrode thickness constant and vary the type of TiO₂ particles used in the paste. This was because DSC devices are tending towards thinner electrodes as the molar extinction coefficient (ϵ) of dyes increase and because solid state devices require thinner electrodes. Thus, two different pastes have been studied in these devices; in house prepared P25-ethyl cellulose-terpineol paste which is denoted P25 in Table 1 and a commercial TiO₂ paste (DSL18NR-T from Dyesol Ltd) which is denoted NRT in Table 1. The data for the TiO₂-only films P25 sintered at 450 °C can be used as a baseline for the other devices. Thus, Device A for P25-only shows η of 4.4% with J_{sc} of 9.01 mA cm⁻² and V_{oc} of 0.71 V. By comparison, Device B gives a better performance ($\eta = 5.0\%$) mainly due to an improvement in J_{sc} up to 9.80 mA.cm⁻². This is ascribed to the DSL18NR-T paste containing smaller, nanoparticulate anatase TiO₂ particles leading to higher dye loading (see ESI Fig. 4). In addition the DSL18NR-T paste contains no rutile phase whilst P25 does which is known to produce less efficient DSC devices³⁶. The DSL18NR-T paste has also been optimized for DSC devices.

For the P25/peroxide films sintered at 450 °C, the highest efficiencies are observed for the ZnO₂ treated pastes. Thus, for P25/ZnO₂ (Device E) $\eta = 4.4\%$ which is comparable to the P25-only device (Device A). By comparison, the NRT/ZnO₂ data (Device F) again shows a significant improvement over the P25 and P25/ZnO₂ data with $\eta = 5.7\%$ which is again mainly due to improved J_{sc} . However, the NRT/ZnO₂ device also shows a significant improvement compared to Device B which contains only DSL18NR-T with improved efficiency again related to improved J_{sc} . This is in line with the P25 data which suggests the ZnO₂ provides an additional benefit to the device performance. This may be because the larger ZnO₂ particles may increase light scattering during device operation and/or that the ZnO₂ particles

provide an additional benefit during sintering leading to improved surface area and dye loading. Having established the influence of peroxide on larger devices, some smaller (0.26 cm²) devices were prepared and ultra-fast dyed with N719/SQ1 cocktail solution²⁷ to study the effect of increased J_{sc} on the peroxide photo-electrodes. This showed that device efficiencies of up to $\eta = 7.5\%$ can be achieved from binder-containing paste sintered at 300 °C (Table 1) which is comparable with previous reports for this dye system²⁷. To the best of our knowledge, the performance of these devices is comparable to the highest efficiency devices reported for DSC fabricated using low temperature methods except that the previous reports used binder-free TiO₂ pastes and pressure rather than thermal sintering^{18,19}.

Sintering the photo-electrodes at 300 °C shows the importance of the metal peroxide additions. For example, sintering P25-only devices at 300 °C gives very low η regardless of whether TiCl₄ treatment is used ($\eta < 0.3\%$, Devices G and H); essentially

Table 1 IV data for (1 cm²) N719-dyed DSC devices prepared using P25 or P25/peroxide pastes (10% wt/wt). Efficiencies are reported as mean of 3 devices for each condition \pm error.

Paste	TiCl ₄	η (%)	FF	V_{oc}/V	$J_{sc}/\text{mA cm}^{-2}$
450 °C					
A P25	Yes	4.4 \pm 0.2	0.69	0.71	9.01
B NRT	Yes	5.0 \pm 0.2	0.65	0.79	9.80
C P25/CaO ₂	Yes	3.4 \pm 0.1	0.61	0.78	6.85
D P25/MgO ₂	Yes	3.5 \pm 0.1	0.57	0.78	7.99
E P25/ZnO ₂	Yes	4.4 \pm 0.1	0.73	0.78	7.73
F NRT/ZnO ₂	Yes	5.7 \pm 0.2	0.72	0.77	10.43
300 °C					
G P25	Yes	0.3	0.61	0.58	0.82
H P25	No	0.0	0.34	0.02	0.20
I P25/CaO ₂	Yes	3.2 \pm 0.2	0.55	0.79	7.32
J P25/MgO ₂	Yes	3.5 \pm 0.1	0.53	0.78	8.32
K P25/ZnO ₂	Yes	4.1 \pm 0.2	0.72	0.77	7.51
L P25/ZnO ₂	No	1.1 \pm 0.0	0.60	0.74	2.53
M NRT/ZnO ₂	Yes	5.7 \pm 0.1	0.71	0.76	10.62
N NRT/ZnO ₂	No	0.0 \pm 0.0	0.00	0.01	0.02
O [†] NRT/ZnO ₂	Yes	7.5 \pm 0.3	0.67	0.84	13.40

[†]Cocktail dyed (N719/SQ1) 0.26 cm² device

resulting in non-functional devices. Sintering DSL18NR-T pastes which do not contain ZnO₂ at 300 °C produces similar device performances; i.e. no efficiency (data not shown). By comparison, sintering P25/metal peroxide films at 300 °C shows similar device performance data to the respective 450 °C sintered films. The highest efficiency for these devices is again observed for P25/ZnO₂ compared to P25/CaO₂ or P25/MgO₂ (Device J *versus* Devices H and I).

The data also show the importance of TiCl₄ treatment for the metal peroxide-containing films. For P25/ZnO₂ pastes, the addition of a TiCl₄ treatment increases η from 1.1% (Device L, no TiCl₄) to 4.1% (Device K, with TiCl₄). For DSL18NR-T/ZnO₂

pastes, the effect is even more pronounced with zero η without TiCl₄ treatment (Device N) and $\eta = 5.7\%$ with TiCl₄ (Device M). For DSL18NR-T, it is hard to compare the data as the absence of TiCl₄ produces a non-functional device. However, for the P25/ZnO₂ devices, the main reason is J_{sc} . This effect is ascribed to the TiCl₄ treatment hydrolyzing onto the photo-electrode surface producing a more coherent TiO₂ surface for dyeing. Indeed, it is known that TiCl₄ treatment has little influence on high temperature sintered devices where all organic matter has been removed and the particles are thermally well sintered together. However, here the value of the TiCl₄ effectively repairing photo-electrode defects can be seen. The differences in performance between the P25 and DSL18NR-T pastes may reflect different paste additives which make it more difficult to remove all organic matter from the commercial paste at 300 °C. To illustrate the importance of J_{sc} , Fig. 4 shows EQE_{max} for N719 at 530 nm for a P25 device sintered at 450 °C. By comparison for films sintered at 300 °C, the P25/ZnO₂ device shows EQE of 45% at 530 nm whilst the equivalent P25-only device shows EQE < 5%. Finally, the data for NRT/ZnO₂ sintered at 300 °C (Device M) shows very similar data to the equivalent device sintered at 450 °C) with $\eta = 5.7\%$; again an improvement over the NRT-only device sintered at 450 °C (Device B).

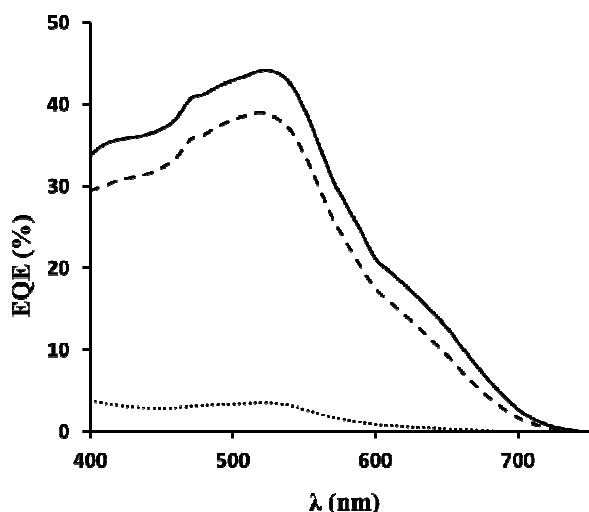


Fig. 4 EQE for P25 films sintered at 300 °C (dotted line), 450 °C (dashed line), and P25/ZnO₂ (solid line) sintered at 300 °C for 30min. All films TiCl₄ treated and dyed with N719.

Transient photovoltage and photocurrent decay measurements have been used to further study the influence of sintering temperature, TiCl₄ treatment and ZnO₂ addition to devices (Fig. 5 and ESI Fig. 5). The data show significantly longer recombination lifetimes for all TiCl₄ treated photo-electrodes compared to their non-TiCl₄ treated analogues. For P25 devices, there is no difference in the transport kinetics which suggests that any increase in J_{sc} observed as a result of TiCl₄ treatment can be attributed to a downward shift in the conduction band as observed in³⁷. For the 300 °C sintered devices however, an apparent decrease in transport kinetics, due to TiCl₄ treatment, may indicate a change in trap density additional to the negative CB shift that is commonly observed as a result of TiCl₄ treatment.

The large decrease in recombination rate observed in devices made with ZnO₂ in the paste suggests that the ZnO₂ performs a different role to TiCl₄ in the devices and supports our assertion that the peroxide assists binder combustion and the removal of residual organic material which otherwise acts as recombination sites. The data also show that the 450 °C sintered P25 device without ZnO₂ or TiCl₄ treatment, shows comparable recombination lifetimes to TiCl₄-treated devices suggesting that TiCl₄ treatment does not significantly affect recombination processes for well-sintered TiO₂-only photo-electrodes which is in line with many literature reports. However, recombination lifetimes shorten for the 450 °C sintered ZnO₂/P25 device without TiCl₄ treatment but are shortest for all the 300 °C sintered devices which have not been TiCl₄ treated. These data confirm that both ZnO₂ and TiCl₄ treatment are required for low temperature sintering to achieve adequate recombination lifetimes for effective charge extraction. Overall, these data show that low temperature sintering of binder-containing TiO₂ pastes is possible and with careful control to minimize any over-sintering of the TiO₂ surface can lead to enhanced short-circuit currents. The later materials characterisation work reported in this paper has sought to understand the reasons for these observations.

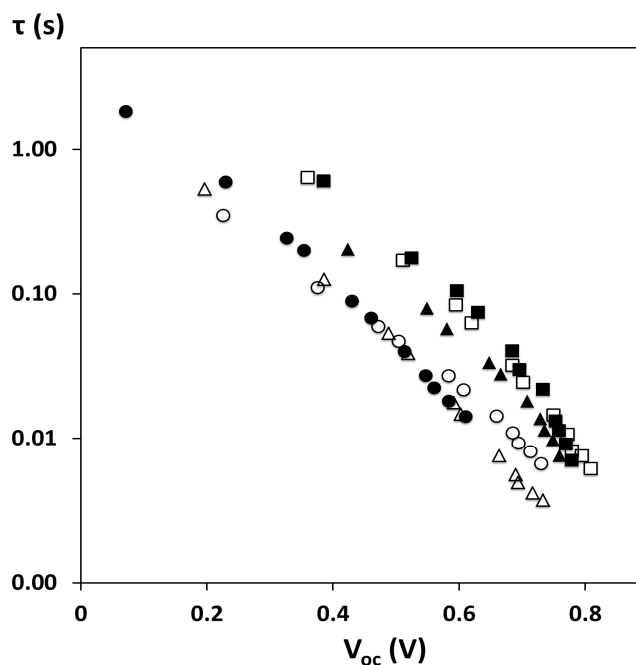


Fig. 5 Recombination lifetime τ versus V_{oc} for devices sintered at 450 °C - ■ P25 with TiCl₄; ▲ P25 no TiCl₄ or at 300 °C - ○ P25 with TiCl₄; △ P25 no TiCl₄; □ ZnO₂/P25 with TiCl₄; ● ZnO₂/P25 no TiCl₄.

Studies of varying the paste ZnO₂ loading from 5 to 25% shows that lower ZnO₂ loading (5-10%) gives the best device performance (see ESI Table 1). This is mainly due to reduced J_{sc} as the metal peroxide loading increases which is ascribed to lower dye loadings arising from increased proportion of lower surface area ZnO₂ particles. Studies of extending the sintering time at 300 °C from 30min to 120min (see ESI Table 2) also show a slight negative impact on device efficiency due to slight reductions in J_{sc} and V_{oc} . These changes probably reflect increased interactions

between the zinc oxide and TiO₂ phases with time which may lead to a loss of surface area and potentially surface doping of each phase into the other.

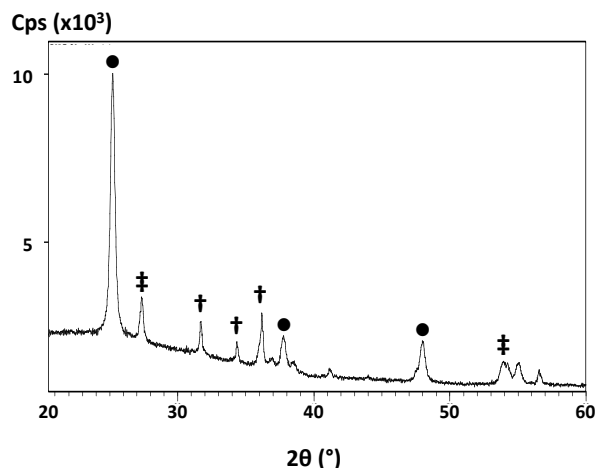


Fig. 6 X-ray diffraction pattern of P25/ZnO₂ film sintered at 300 °C showing • anatase TiO₂, ◼ rutile TiO₂ and ▲ ZnO

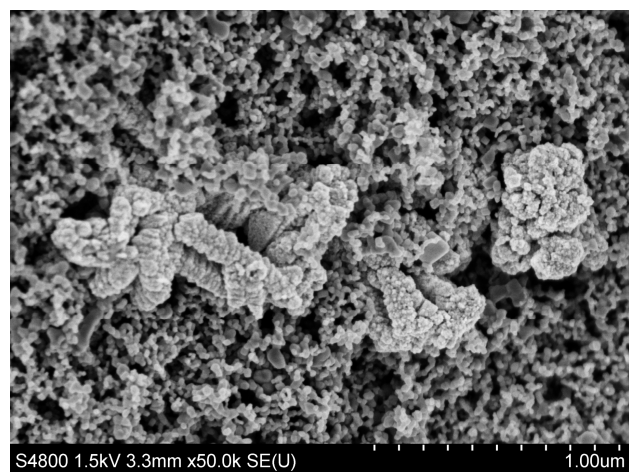


Fig. 7 Scanning electron micrographs of ZnO₂-containing P25 films sintered at (top) 450 °C and (bottom) 300 °C

Materials Characterisation

The aim of this part of the work has been to try to understand how the addition of metal peroxides to TiO₂-ethyl cellulose pastes affects the phases and morphology of the resulting metal oxides. Their surface chemistry has also been studied using BET and dye loading isotherms because of the strong correlation between device performance and J_{sc} . Thus, a key aim of this work has been to understand if the completion of sintering and any presence of residual organic matter is linked to surface area and dye loading. Unless otherwise stated, the data for P25-ethyl cellulose pastes containing 10% ZnO₂ (by wt.) are presented these pastes gave rise to the most efficient DSC devices.

Firstly, looking at the structural phases present, XRD data show that all the films contain anatase³⁸ and rutile³⁹ TiO₂ phases in approximately 4:1 ratio as expected for P25. The data for a sintered P25/ZnO₂ film (Fig. 6) shows additional peaks at 31.7° and 34.4° 2θ, which can be attributed to ZnO⁴⁰ resulting from the decomposition of ZnO₂. The data for P25/CaO₂ or P25/MgO₂ films were essentially identical to the P25-only film with no evidence for the formation of a second metal oxide phase which suggests that the CaO₂ or MgO₂ form amorphous products on decomposition (see ESI Fig. 6). The P25-only XRD data also show slight narrowing of the diffraction lines (see ESI Figs. 6 and 7) for films sintered at 450 °C compared to 300 °C in line with increased crystallinity and inter-particle necking. Interestingly, a similar but subtle effect is seen for the P25/peroxide films sintered at 300 °C. It is difficult to identify the reasons for this with absolute confidence because XRD measures an “average” across the whole sample. However, this might reflect the generation of localized heat during peroxide decomposition as the TGA shows this is an exothermic process. In turn, this might increase TiO₂ crystallinity and /or might reflect increased inter-particle interactions leading to increased crystallite size.

SEM data (Fig. 7) clearly show two different types of particle interspersed within the film. The majority of particles are *ca.* 25 nm and EDX analysis (see ESI Fig. 8) shows the presence of Ti and O confirming these as P25 TiO₂ nanoparticles (Fig. 7 - top). The data also show larger irregularly-shaped agglomerations of particles which are 100-300 nm in size and which EDX data show contain Zn and O confirming these to be the ZnO particles arising from the thermal decomposition of ZnO₂. Interestingly, the surface morphology of particles appears different dependent on the sintering temperature. Thus, after sintering at 450 °C, the surface appears smooth and the particles singular whilst the 300 °C sintered particles are larger (120-600 nm), have a much more irregular surface and appear to be made up of many smaller particles. This suggests that, whilst the TGA data show that the loss of O₂ from the ZnO₂ occurs rapidly at *ca.* 200 °C, the atomic rearrangement into a more ordered ZnO structure is not complete after 30min at 300 °C.

Sorption data have been measured either using N_{2(g)} sorption data at -196 °C fitted to the BET model isotherm or using N719 dye solutions sorbed at 22, 40 or 50 °C which have been fitted to model Langmuir or Freundlich isotherms. The dye uptake data have been measured using relatively low initial dye concentrations passively dyed and at equilibrium to study the effects of photo-electrode composition (\pm ZnO₂) and sintering

conditions (300 vs 450 °C) rather than to optimise sensitization. Thus, fast dyeing²⁷ higher initial dye concentrations would be expected to show different responses but that is beyond the scope of this paper. P25/ZnO₂ films were chosen as these devices show the best device responses compared to the P25 or other P25/peroxide films (Table 1).

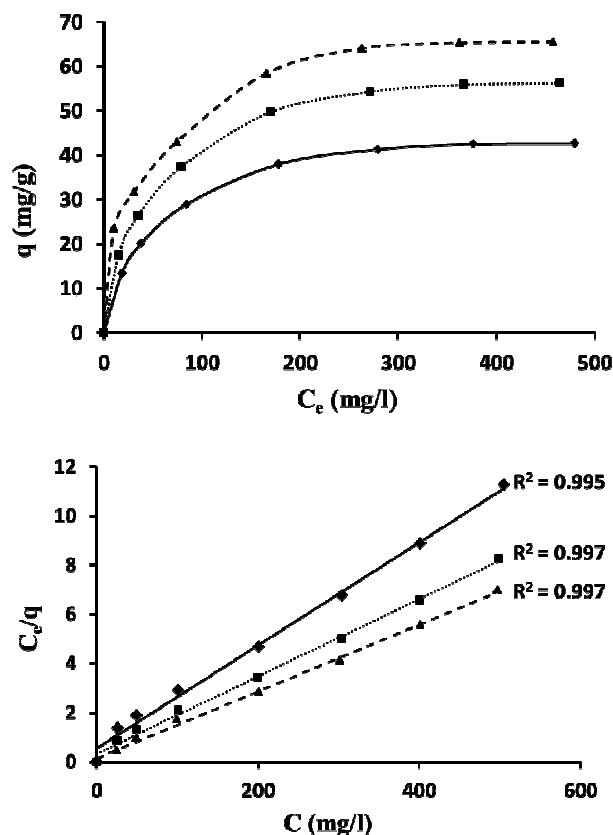


Fig. 8 (Top) adsorption isotherms for N719 dyed at 22 °C onto (solid line, diamonds) P25 sintered at 450 °C; (dotted line, squares) P25/ZnO₂ sintered at either 450 °C or (dashed line, triangles) at 300 °C and (bottom) the same data fitted to Langmuir isotherms.

The N₂ sorption BET data show a surface area of 54 m² g⁻¹ for P25 sintered a 300 °C which drops to 45 m²g⁻¹ after sintering at 450 °C. This is expected because one aim of the raising the temperature to 450 °C is to sinter particles together and create inter-particle necking. This can only be achieved if the TiO₂ surface atoms become mobile. If this occurs, then surface tension will provide a driving force towards smoothing the surface to the lowest surface area. In this case, 450 °C is not sufficient to complete this process but is sufficient to sinter the particles together. For the P25/ZnO₂ data, a similar trend is observed but with a surface area of 51 m²g⁻¹ at 300 °C and 42 m²g⁻¹ at 450 °C. The situation is complicated for these samples partly because they contain a mixture of TiO₂ particles along with a smaller number of ZnO particles which have resulted from the decomposition of ZnO₂ but also because the surface area measurement is an average across the whole. Looking at neat ZnO₂ powder first, this has a surface area of 14 m²g⁻¹ at RT which increases slightly to 18 m²g⁻¹ after sintering at 300 °C but

drops to 7.8 m²g⁻¹ at 450 °C. These trends are typical for a material such as ZnO₂ which releases gas during decomposition as this effectively bursts out of the material creating increased surface area during the process⁴¹. However, the resultant ZnO particles sinter rapidly as the temperature is increased further to 450 °C resulting in a subsequent loss of surface area. Thus, whilst the “average” surface area for P25/ZnO₂ might be expected to be slightly lower to reflect the addition of lower surface area ZnO₂ particles, it is not possible to separate out what is happening to the surface of the TiO₂ particles alone. In addition, N₂ will physisorb to residual organic matter and also include this surface area in the data whilst N719 dye will only chemisorb to “free” metal oxide surfaces. Finally, N₂ is much smaller than N719 so their sorption characteristics will be different. Hence, although the BET data are useful in highlighting trends between organic matter containing under-sintered samples and over-sintered samples (where surface area begins to be lost), dye loading data have been measured and analysed in some detail to provide the most accurate picture of metal oxide surface for dye binding.

The dye sorption data show relatively higher dye sorption at low initial dye concentration. However, as the initial dye concentration increases, dye sorption increases but to a relatively lesser extent until the data reach a plateau (Fig. 8 - top). This is expected as there are a fixed number of sorption sites in the metal oxide films and, as these become increasingly filled fewer free sites remain, and greater dye concentrations are required to partition more dye onto the surface. However, in these measurements, the dye concentration decreases throughout the experiment as dye adsorbs until equilibrium is reached between the remaining free sites and the remaining dye concentration. Thus, if dye concentration is proportional to the driving force for dye sorption and this drops throughout the sorption process, initial dye concentration should be predictive of final dye loading.

Table 2 Parameters derived from Langmuir isotherms for N719 dyed at 22, 40 or 50 °C onto P25 sintered at 450 °C or onto P25/ZnO₂ films sintered at 300 or 450 °C

Paste	Dyeing temp. (°C)	q _m (mg/g)	K _L (l/mg)	R _L	R ²
P25 (450 °C)	22	47.5	0.021	0.088	0.999
	40	76.6	0.022	0.082	0.998
	50	85.9	0.030	0.050	0.998
P25/ZnO ₂ (450 °C)	22	62.1	0.023	0.081	0.999
	40	88.4	0.029	0.064	0.998
	50	106.3	0.038	0.050	0.997
P25/ZnO ₂ (300 °C)	22	70.9	0.029	0.064	0.997
	40	94.8	0.040	0.048	0.997
	50	116.2	0.044	0.043	0.997

Comparing the two isotherm models, the R² values are consistently higher when the data are fitted to the Langmuir isotherm (R² > 0.997) compared to the Freundlich isotherm (R² 0.962-0.983); see ESI Fig. 9-11 and ESI Tables 3-6. The

Langmuir model assumes monolayer sorption of adsorbates onto identical sites in separate sorption events whilst the Freundlich model assumes that adsorption takes place on heterogeneous surfaces and is not restricted to monolayer sorption³³. On the basis of the higher correlations, the Langmuir data have been used to analyse dye uptake using P25 films sintered at 450 °C as a control to compare to P25/ZnO₂ films sintered at either 450 or 300 °C.

Firstly comparing P25 and P25/ZnO₂ data sintered at 450 °C, the values for adsorption capacity (q_m) are consistently higher for the P25/ZnO₂ films which is in line with higher J_{sc} in these devices (Table 2). This is despite the slightly lower surface area for the P25/ZnO₂ films measured by N₂ sorption. As discussed previously, the N₂ BET data measures an “average” surface area of the entire sample surface (TiO₂, ZnO and any residual organic matter). However, we expect the dye sorption data to only measure a monolayer of N719 dye chemisorbed to any available metal oxide surfaces. Thus, we believe the increased dye loading in P25/ZnO₂ samples reflects improved removal of residual organic matter from the metal oxide surfaces that improves the metal oxide surfaces for dye uptake. However, the device efficiency data (ESI Table 1) show that increasing the ZnO₂ loading within the films from 5 to 15 to 25% reduces device performance. This suggests that the increases in dye uptake are associated with improvements to the surface of TiO₂ particles. This is in line with earlier assertions that the main role of ZnO₂ is to release oxygen and heat to aid binder combustion which removes organic matter and increases TiO₂ surface area for dye binding.

The data in Table 2 also show that adsorption capacity is higher for P25/ZnO₂ films sintered at 300 °C than P25 or P25/ZnO₂ sintered at 450 °C. This is to be expected based on the higher BET surface area for P25/ZnO₂ sintered at 300 °C. However, as discussed previously, the situation is complicated because the BET data is an average of all the material in the sample. The increased dye uptake for P25/ZnO₂ at 300 °C does suggest that the presence of ZnO₂ results in greater removal of residual organic matter from metal oxide surfaces (which in this sample must be dominated by the much more abundant TiO₂ particles). In addition, higher BET surface area and increased dye loading after 300 °C sintering suggests that, as long as residual binder can be removed at lower temperature, the metal oxide particles lose less surface area than if sintered at 450 °C. However, this benefit can only be realised in increased dye loading if combustion agent such as ZnO₂ is added to help combust the residual binder. This beneficial influence on dye loading has not been realised before because it has not been previously been possible to sinter binder-containing pastes at low temperature.

Table 2 also shows that the N719 adsorption capacity increases on all films with dyeing temperature which suggests an endothermic adsorption process. In practice, solvent volatility limits dyeing temperature and so these data have only been measured up to 50 °C. Low R_L values indicate favourable dye uptake³⁰. The data show that R_L values decrease with increasing dyeing temperature and also across the series P25 450 °C > P25/ZnO₂ (450 °C) > P25/ZnO₂ (300 °C). Thus, P25/ZnO₂ films

sintered at 300 °C and dyed at 50 °C show the most favourable N719 uptake in line with the highest N719 adsorption capacity. This is in line with the J_{sc} and η data which suggests that, as expected, J_{sc} is linked to dye loading (Table 1).

Conclusions

The data show that, for the first time, binder-containing pastes can be sintered at low temperature by using metal peroxide combustion promoters. This has the advantage that metal peroxides are low cost powders which are safe and easy to use within commonly used paste formulations. The most effective metal peroxide when using ethyl cellulose binder-containing pastes is ZnO₂ which is believed to be because ZnO₂ decomposes at similar temperatures to ethyl cellulose combustion so that the oxygen released during this process enhances binder combustion and removal as CO_{2(g)} at lower temperature. In addition, the by-products of ZnO₂ decomposition are relatively large particles of ZnO which may enhance light scattering within the device whilst not limiting the device because ZnO is used as a photo-anode material in DSC devices in its own right.

The sorption data show the importance of considering BET surface area data arising from multi-layer N₂ physisorption as an average of the whole sample surface area whilst dye loading data relate to chemisorbed dye monolayers. Furthermore, dye loading data after sintering at lower temperatures show, for the first time, that this can actually give rise to higher dye loadings which is linked to the removal of residual binder at lower temperatures along with a reduction in the loss of metal oxide surface area associated with 450 °C sintering. This suggests that sintering at 450 °C actually slightly over-sinters the TiO₂ resulting in a loss of surface area and lower dye loading. However, it remains important to remove the vast majority (and ideally all) of the organic binder in order to maximize the number of dye binding sites and resulting J_{sc} . Thus, a general model of sintering would be to sinter at the lowest possible temperature to remove organic material, optimize dye loading and enable inter-particle connections to form to ensure the films are mechanically robust.

Acknowledgements

We gratefully acknowledge Iraqi Govt. support for DKM, ERDF-WG LCRI funding for SPARC (AC, EWJ, CC), EPSRC SPECIFIC funding (MLD) and Sêr Cymru funding (PJH), Drs Graham Ormondroyd and Simon Curling in the Biocomposites Centre for BET measurements and NSG for supply of TECTM glass to the SPARC consortium.

Notes and references

^a School of Chemistry, Bangor University, Gwynedd LL57 2UW UK. E-mail: p.j.holliman@bangor.ac.uk Fax: +44 (0)1248 370528; Tel: +44 (0)1248 382375

^b SPECIFIC, College of Engineering Swansea University, Baglan Bay Innovation and Knowledge Centre, Port Talbot SA12 7AZ (UK)

[†] Electronic Supplementary Information (ESI) available: [details of any supplementary information available should be included here]. See DOI: 10.1039/b000000x/

¹ B. O'Regan and M. Grätzel, *Nature*, 1991, **353**, 24.

- ² C.J. Barbé, F. Árendse, P. Comte, M. Jirousek, F. Lenzmann, V. Schlover and M. Grätzel, *J. Am. Ceram. Soc.*, 1997, **80**, 3157-3171.
- ³ N. Park, J. van de Lagemaat and A. Frank, *J. Phys. Chem. B*, 2000, **104**, 8989-8994.
- ⁴ M. Grätzel, *J. Sol-gel Sci. Technol.*, 2001, **22**, 7-13.
- ⁵ L.M. Gonçalves, V. de Zea Bermudez, H.A. Ribeiro and A.M. Mendes, *Energy Environ. Sci.*, 2008, **1**, 655-667.
- ⁶ P.J. Holliman, M.L. Davies, A. Connell, M.J. Carnie and T.M. Watson, in *Functional Materials for Energy Applications*, Eds. J.A. Kilner, S. J. Skinner, S.J.C. Irvine, P.P. Edwards 2012, Woodhead Publ., Cambridge. ISBN-13: 978 0 87509 059 1.
- ⁷ J. Nelson, *Phys. Rev. B*, 1999, **59**, 15374-15380.
- ⁸ S. Ito, N.-L. Cevey Ha, G. Rothenberger, P. Liska, P. Comte, S.M. Zakeeruddin, P. Péchy, M.K. Nazeeruddin and M. Grätzel, *Chem. Commun.*, 2006, 4004-4006.
- ⁹ K. Miettunen, J. Halme and P. Lund, *WIREs Energy Environ.*, 2013, **2**, 104-120.
- ¹⁰ Y. Kijitori, M. Ikegami, T. Miyasaka, *Chem. Lett.*, 2007, **36**(1), 190-191.
- ¹¹ F. Pichot, J.R. Pitts and B.A. Gregg, *Langmuir*, 2000, **16**, 5626-5630.
- ¹² T.M. Paronyan, A. Kechiantz and M. Lin, *Nanotech.*, 2008, **19**, 115201.
- ¹³ D. Zhang, T. Yoshida, K. Furuta and H. Minoura, *J. Photochem. Photobiol. A: Chem.*, 2004, **164**, 159-166.
- ¹⁴ C. Li, Y. Lin, X. Li, Z. Wang, Y. Ma, X. Zhou, S. Feng and X. Xiao, *Chin. Sci. Bull.*, 2005, **50**, 1449-1452.
- ¹⁵ Y. Xiao, J. Wu, Q. Li, G. Xie, G. Yue, H. Ye, Z. Lan, M. Huang and J. Lin, *Chin. Sci. Bull.*, 2010, **55**, 980-985.
- ¹⁶ D. Gutiérrez-Tauste, I. Zumeta, E. Vigil, M. A. Hernández-Fenollosa, X. Domènech and J.A. Ayllón, *J. Photochem. Photobiology A: Chemistry*, 2005, **175**, 165-171.
- ¹⁷ D. Zhang, T. Yoshida, T. Oekermann, K. Furuta and H. Minoura, *Adv. Func. Mats.*, 2006, **16**, 1228-1234.
- ¹⁸ T. Yamaguchi, N. Tobe, D. Matsumoto, T. Nagai, H. Arakawa., *Solar Energy Mat Solar Cells*, 2010, **4**, 812-816
- ¹⁹ T. Yamaguchi, N. Tobe, D. Matsumoto, H. Arakawa, *Chem. Commun.*, 2007, 4767-4769
- ²⁰ S. Senthilarasu, T.A. Nirmal Peiris, J. Garcia-Canadas and K.G. Ubul Wijayantha, *J. Phys Chem. C*, 2012, **116**, 19053-19061.
- ²¹ A.G. Agrios and A. Hagfeldt, *J. Phys. Chem. C*, 2008, **112**, 10021-10026.
- ²² . Li, J. Li, N. Wang, C. Lin and L. Zhang, *J. Photochem. Photobiol. A: Chemistry*, 2008, **195**, 247-253.
- ²³ T. Kado, M. Yamaguchi, Y. Yamada and S. Hayase, *Chem. Lett.*, 2003, 1056-1057.
- ²⁴ H. Kim, R. Auyeung, M. Ollinger, G. Kushto, Z. Kafafi and A. Piqué, *Appl. Physics A: Mats. Sci. Process.*, 2006, **83**, 73-76.
- ²⁵ S. Uchida, M. Tomiha, H. Takizawa and M. Kawaraya, *J. Photochem. Photobiol. A: Chem.*, 2004, **164**, 93-96.
- ²⁶ Y. Kim, B.J. Yoo, R. Vittal, Y. Lee, N.-G. Park and K.-J. Kim, *J. Power Sources*, 2008, **175**, 914-919.
- ²⁷ P.J. Holliman, M.L. Davies, A. Connell, B. Vaca Velasco and T.M. Watson, *Chem. Comm.*, 2010, **46**, 7256-7258.
- ²⁸ P.R.F. Barnes, K. Miettunen, X. Li, A.Y. Anderson, T. Bessho, M. Grätzel and B.C. O'Regan, *Adv. Mater.*, 2013, **25**(13), 1881-922
- ²⁹ P. Joshi, L. Zhang, D. Davoux, Z. Zhu, D. Galipeau, H. Fong and Q. Qiao, *Energy & Env. Sci.*, 2010, **3**, 1507-1510.
- ³⁰ M. Alkan, O. Demirbas and M. Dogan, *Fres. Env. Bull.*, 2004, **13**, 1112-1121.
- ³¹ J. Fan, W. Cai and J. Yu, *Chem. – Asian J.*, 2011, **6**, 2481-2490.
- ³² P.J. Holliman, B. Vaca Velasco, I. Butler, M. Wijdekop and D.A. Worsley, *Int. J. Photoenergy*, 2008, 1-8.
- ³³ H.J. Snaith, *Energy Env. Sci.*, 2012, **5**, 6513.
- ³⁴ S. Ito, P. Chen, P. Comte, M.K. Nazeeruddin, P. Liska, P. Péchy, M. Grätzel, *Progr. Photovolt.: Res. Appl.*, 2007, **15**, 603-612.
- ³⁵ Y. Yamamoto, M. Kawaraya, H. Segawa, S. Uchida, J. Kano, F. Saito, K. Tsujimoto, T. Saito, S. Ito, *Chem. Lett.*, 2011, **40**, 1220-1222.
- ³⁶ N. Park, J. van de Lagemaat and A. Frank, *J. Phys. Chem. B*, 2000, **104**, 8989-8994.
- ³⁷ B.C. O'Regan, J.R. Durrant, P.M. Sommeling and N.J. Bakker, *J. Phys. Chem. C*, 2007, **111**, 14001-14010.
- ³⁸ JCPDS 01-071-1168 (Anatase – TiO₂)
- ³⁹ JCPDS 01-071-0650 (Rutile – TiO₂)
- ⁴⁰ JCPDS 00-003-0888 (ZnO)
- ⁴¹ T. Baird, K. Campbell, P.J. Holliman, R. Hoyle, D. Stirling and D.P. Williams, *J. Chem. Soc. (Faraday Trans.)*, 1995, **91**, 3219-3230.

The first report of low temperature thermal sintering of binder-containing TiO_2 pastes giving $\eta = 7.5\%$ using metal peroxide combustion promoters.

